Report

Current Biology

Sun Navigation Requires Compass Neurons in *Drosophila*

Highlights

- Flying *Drosophila* can navigate a straight path using the position of the sun
- Flies can remember their sun compass heading from one flight to the next
- Sun position is encoded by compass cells within the central complex of the brain
- Genetic silencing of compass cells within the brain interferes with sun navigation

Authors

Ysabel Milton Giraldo, Katherine J. Leitch, Ivo G. Ros, Timothy L. Warren, Peter T. Weir, Michael H. Dickinson

Correspondence

flyman@caltech.edu

In Brief

Giraldo et al. find that flying *Drosophila* navigate by holding the sun at a fixed position, which they remember across successive flights. Imaging experiments reveal a class of neurons in the brain that track the motion of the sun. When these cells are silenced, flies no longer adopt and maintain arbitrary headings but instead exhibit phototaxis.

Giraldo et al., 2018, Current Biology *28*, 2845–2852
September 10, 2018
https://doi.org/10.1016/j.cub.2018.07.002

CellPress

Current Biology
Report

CellPress

Sun Navigation Requires Compass Neurons in *Drosophila*

Ysabel Milton Giraldo,[1] Katherine J. Leitch,[1] Ivo G. Ros,[1] Timothy L. Warren,[1,2,3] Peter T. Weir,[1] and Michael H. Dickinson[1,4,*]
[1]Division of Biology and Biological Engineering, California Institute of Technology, Pasadena, CA 91125, USA
[2]Institute of Neuroscience, University of Oregon, Eugene, OR 97401, USA
[3]Department of Botany and Plant Pathology, Oregon State University, Corvallis, OR 97331, USA
[4]Lead Contact
*Correspondence: flyman@caltech.edu
https://doi.org/10.1016/j.cub.2018.07.002

SUMMARY

Despite their small brains, insects can navigate over long distances by orienting using visual landmarks [1], skylight polarization [2–9], and sun position [3, 4, 6, 10]. Although *Drosophila* are not generally renowned for their navigational abilities, mark-and-recapture experiments in Death Valley revealed that they can fly nearly 15 km in a single evening [11]. To accomplish such feats on available energy reserves [12], flies would have to maintain relatively straight headings, relying on celestial cues [13]. Cues such as sun position and polarized light are likely integrated throughout the sensory-motor pathway [14], including the highly conserved central complex [4, 15, 16]. Recently, a group of *Drosophila* central complex cells (E-PG neurons) have been shown to function as an internal compass [17–19], similar to mammalian head-direction cells [20]. Using an array of genetic tools, we set out to test whether flies can navigate using the sun and to identify the role of E-PG cells in this behavior. Using a flight simulator, we found that *Drosophila* adopt arbitrary headings with respect to a simulated sun, thus performing menotaxis, and individuals remember their heading preference between successive flights—even over several hours. Imaging experiments performed on flying animals revealed that the E-PG cells track sun stimulus motion. When these neurons are silenced, flies no longer adopt and maintain arbitrary headings relative to the sun stimulus but instead exhibit frontal phototaxis. Thus, without the compass system, flies lose the ability to execute menotaxis and revert to a simpler, reflexive behavior.

RESULTS

To follow a straight course, animals must maintain a constant heading relative to a fixed, distant landmark, a strategy termed "menotaxis." We tested the hypothesis that *Drosophila* can perform menotaxis using the sun by placing tethered wild-type female flies in a flight simulator and presenting an ersatz sun stimulus (Figure 1A). The fly was surrounded by an array of LEDs, on which we presented either a single 2.4° bright spot on a dark background or a 15°-wide dark vertical stripe on a bright background. Given previous studies on other species [4, 15, 16], we expected that flies would react to our small bright spot as they would to the actual sun; thus, we called it a "sun stimulus." Experiments were conducted in closed loop, so that the difference in stroke amplitude between the fly's two wings determined the angular velocity of the stimulus [12]. Flies generally maintained the dark stripe in front of them (Figures 1C and 1D), a well-characterized behavior termed "stripe fixation" [21–23]. However, when presented with the sun stimulus, individual flies adopted arbitrary headings, thus exhibiting menotaxis (Figures 1B and 1D). We quantified how well flies maintained a heading by calculating vector strength, which is the magnitude of the mean of all instantaneous unit heading vectors for the entire flight. A vector strength of 1 would indicate that a fly held the stimulus at the exact same heading during the entire flight bout. Because we tested each individual with both a stripe and sun stimulus, we could compare the flies' performance under the two conditions. We found no correlation between the mean heading exhibited by individual flies during sun menotaxis and stripe fixation ($p = 0.143$; see STAR Methods for details; Figure 1E), suggesting that heading preference for the sun stimulus is independent of the response to a vertical stripe. To ensure that flies' stabilization of the sun stimulus was not an artifact of our feedback system, we also conducted control closed-loop experiments, in which the bright spot was switched off. As expected, the flies exhibited no orientation behavior under this condition, with all vector strength values lower than 0.16 (Figure 1D). Collectively, these experiments indicate that flies are capable of orienting to a small bright spot and that this behavior is distinct from stripe fixation. *Drosophila* can also perform menotaxis using the axis of linearly polarized light [8, 9, 24]. It is not known whether the orientation responses of flies to the sun and polarized light are independent, as they are in dung beetles [25], or linked to create a matched filter of the sky, as they are in locusts [15].

Given that individual flies adopt arbitrary headings with respect to the sun stimulus, we next tested whether they retain a memory of their orientation preference from one flight to the next. We presented flies with the sun stimulus in closed-loop, interrupted flight for a defined interval (5 min, 1 hr, 2 hr, or 6 hr) and

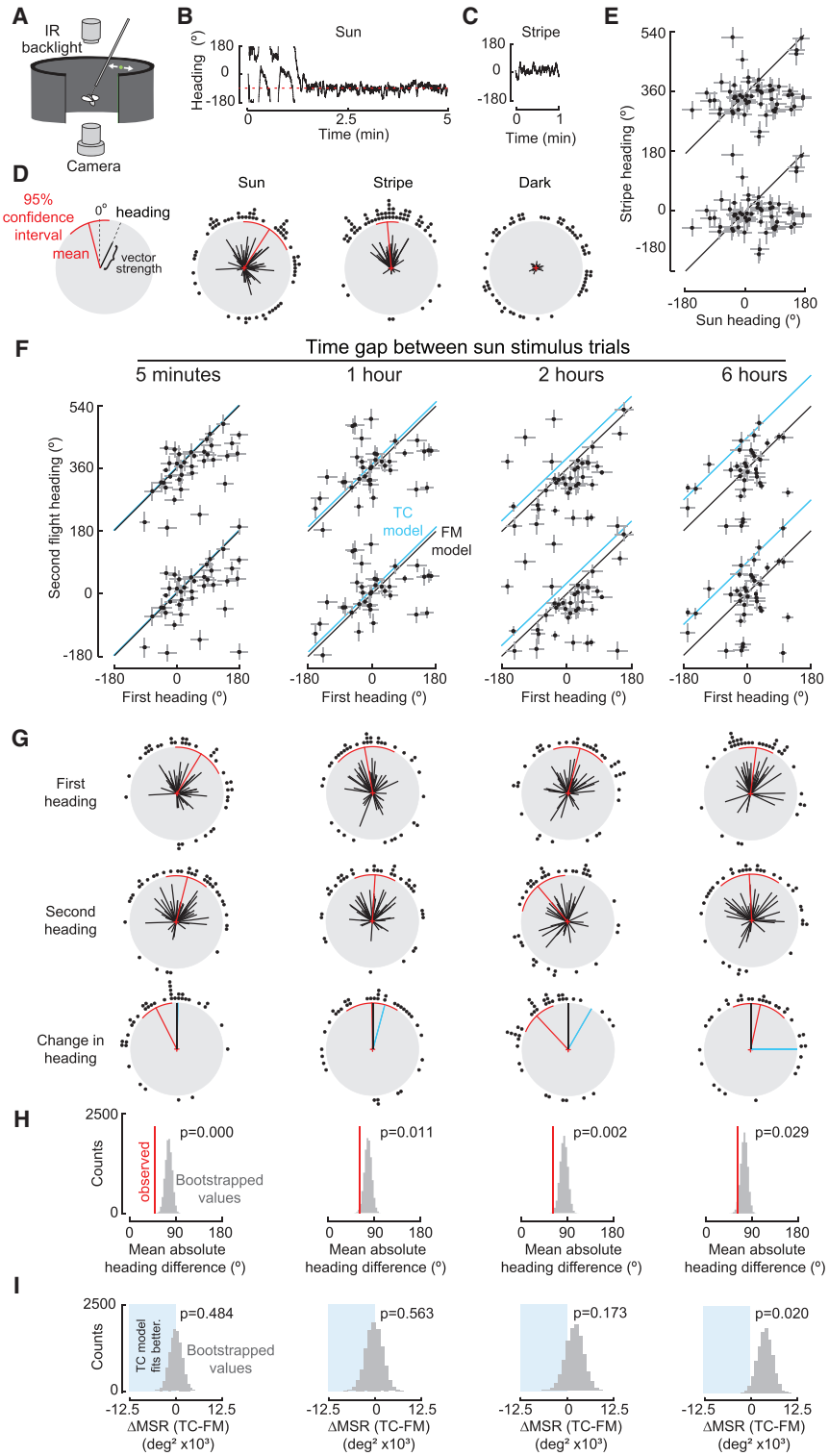

Figure 1. Flies Navigate Using a Sun Stimulus and Retain Memory of Their Heading

(A) A tethered fly, backlit with infrared light, is surrounded by a cylindrical LED display; a single 2.4° spot simulates the sun.

(B) Example trace showing closed-loop behavior. After ~90 s, the fly stabilized the sun stimulus at a heading of −92° (dashed red line).

(C) Heading during a stripe presentation.

(D) Polar representation of data for flies presented with a sun stimulus, with a stripe, and in the dark. Angular position indicates a fly's mean heading; radial distance indicates vector strength. Red line indicates population mean heading with a circular 95% confidence interval; a histogram of mean headings is plotted around each circle. Due to high variance, we could not calculate a 95% confidence interval for the dark data and do not present a population mean heading, as it is not meaningful with such low vector strengths. A Rayleigh test indicates that headings in the dark are uniformly distributed ($p = 0.158$), whereas this test rejects uniformity for all datasets with visual feedback throughout the study ($p < 0.008$ in all cases).

(E) Sun versus stripe headings for data shown in (D). Data are repeated on the vertical axis to indicate their circular nature. Diagonal line indicates identical heading over both trials. Error bars indicate circular variance multiplied by an arbitrary scale factor, 36, for visibility. Distributions of mean headings for the sun and stripe are different (Mardia-Watson-Wheeler, $W = 13.916$, $p = 0.001$).

(F) Heading in first trial plotted against second trial heading for increasing inter-trial intervals; plotting conventions are as in (E). Only flies for which both trials had a vector strength >0.2 are plotted. The black lines again indicate exact correspondence between the first and second sun flight headings, which we refer to as the fixed memory (FM) model. Blue lines indicate the expected shift in headings if flies performed a full time compensation (TC) model, assuming a sun movement of 15° hr^{-1}.

(G) Headings for first and second sun presentations for flies in which both trials had a vector strength greater than 0.2; plotting conventions are as in (D). Note that the first sun trial for the 5-min dataset is the same data as in (D), except with the 0.2 vector strength cutoff applied. The bottom row of plots indicates the change in heading, with black and blue lines indicating expected values for FM and TC models, respectively.

(H) Distribution of 10,000 bootstrapped heading differences between random pairings of first and second trials from (F). Red line indicates mean heading difference of observed data; p value, proportion of resampled differences that are smaller than the observed mean heading difference.

(I) Statistical comparison of FM and TC models. Gray histogram shows the distribution of the difference in mean squared residuals (ΔMSR) between the TC and FM models calculated from 10,000 random samples of 20 data pairs. Blue shading and p values indicate the proportion of subsampled ΔMSRs in which the TC model performed better than the FM model.

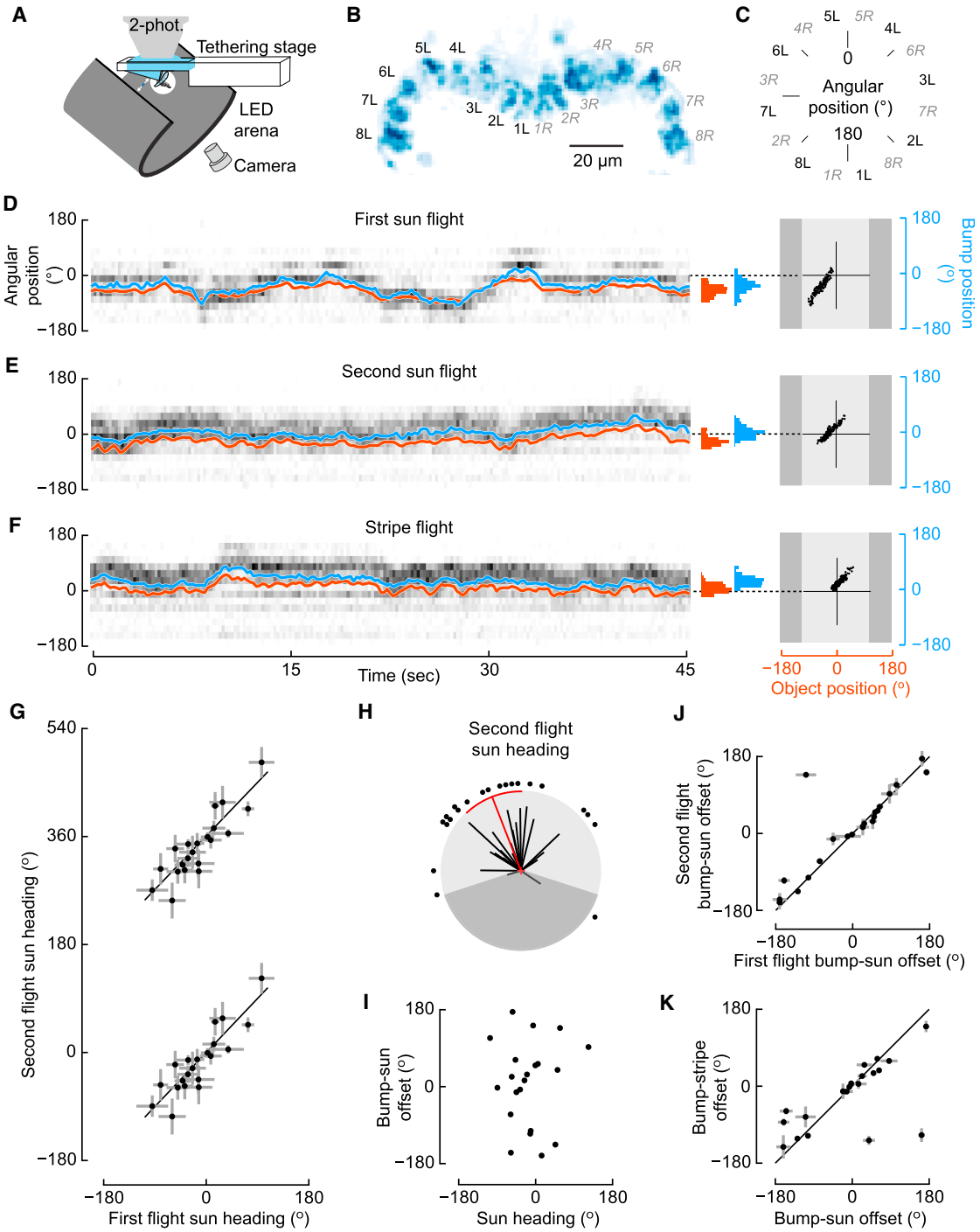

Figure 2. E-PG Neuron Activity Correlates with Both Sun and Stripe Positions

(A) Ca^{2+} imaging schematic.

(B) Glomeruli assignment in protocerebral bridge based on an SD of GCaMP6f fluorescence in E-PG terminals.

(C) Continuous circular representation of angular position based on glomeruli positions in (B).

(D) Example trial from functional imaging experiment. GCaMP6f fluorescence (ΔF/F), shown in grayscale, is plotted in each glomerular position (from C) during 45 s of a sun stimulus presentation. Azimuthal position of the E-PG activity bump (blue trace, computed as in [29]) and sun position (red trace) co-vary. Histograms showing angular distributions for each trace are shown at the right, as are regressions plotting sun position against bump position. The dark gray regions in the regression plots indicate the sectors of the arena in which the stimulus was not visible to the fly.

(E) Same as in (D), but showing data from the second sun presentation.

(F) Same as in (D), but showing data from the stripe presentation.

(G) Heading during the second sun trial plotted against heading in the first sun trial, with a minimum 5-min inter-trial interval (n = 20; plotted as in Figure 1E).

(legend continued on next page)

then again presented the sun stimulus. To provide an independent metric of flight performance, we also presented a stripe under closed-loop conditions for 1 min before the first sun bout and after the second. In all cases, distributions of mean headings for the sun and stripe trials were different (Mardia-Watson-Wheeler test: 5 min, $W = 13.916$, $p = 0.001$; 1 hr, $W = 12.551$, $p = 0.002$; 2 hr, $W = 28.891$, $p = 0.000$; 6 hr, $W = 10.256$, $p = 0.006$), and these results were robust to excluding any trials with vector strengths less than 0.2 (all ps < 0.03). Across inter-flight intervals of 5 min, 1 hr, 2 hr, and even 6 hr, flies tended to remain loyal to their first heading during the second flight (Figures 1F and 1G). If each fly adopted the identical heading in both flights, the mean heading difference would be zero, whereas if there was no correlation in heading from one flight to the next, the mean absolute value of the heading differences would be 90°, provided that the orientations were uniformly distributed. To test whether the consistency in flight-to-flight orientation could arise from chance, we iteratively shuffled pairings of mean heading values of first and second flights 10,000 times and compared the resulting bootstrapped distributions with the mean absolute heading difference of the actual data (Figure 1H). In all cases, the measured mean difference was substantially less than the mean of the bootstrapped values (5 min: 49.8° versus 76.3°; 1 hr: 61.0° versus 77.4°; 2 hr: 62.8° versus 83.8°; 6 hr: 61.4° versus 74.4°). We calculated probability values directly from the proportion of simulations that resulted in a smaller mean absolute angle difference than the observed data (Figure 1H). In all cases, this probability was quite low (5 min: $p = 0.000$; 1 hr: $p = 0.011$; 2 hr: $p = 0.002$; 6 hr, $p = 0.029$). Because the heading value of an individual trial is unreliable when vector strength is low, this analysis was conducted after excluding trials in which the vector strength was less than 0.2 (36% of all trials). However, the probabilities calculated using the entire dataset were also very low, except for the 6-hr gap (5 min: $p = 0.000$; 1 hr: $p = 0.028$; 2 hr: $p = 0.001$; 6 hr: $p = 0.084$). Collectively, these results suggest that headings are not selected at random with each subsequent takeoff but, rather, that flies remember their headings from previous flights for up to 2 hr and possibly longer. A similar result was found for the orientation responses to linearly polarized light, although only a 5-min time gap was tested [8]. Fully determining the mechanisms by which flies attain their initial heading preference (i.e., genetic versus developmental versus learning) requires experiments that are beyond the scope of this study.

Monarch butterflies and bees, which use a sun compass for migration and foraging, respectively, exhibit time compensation so that their orientation preference adjusts for the azimuthal motion of the sun through the sky. The time course of our two-flight experiments allowed us to test whether flies also utilize a time-compensated sun compass. The blue diagonal lines in Figure 1F plot the prediction of a time-compensated (TC) model, assuming a sun procession of $15° \text{ hr}^{-1}$ [26], whereas the black lines indicate the prediction of a fixed memory (FM) model in which the headings of the first and second flights are identical. Visual inspection suggests that the FM model predicts the data distributions better than the TC model. This impression was confirmed by a statistical analysis in which we randomly resampled 20 values 10,000 times, in each case calculating the difference in the mean square residual (MSR) values for the TC and FM models (Figure 1I). We then used the bootstrapped distributions to determine the probability that the TC model predicted the data better than the FM model (5 min: $p = 0.484$; 1 hr: $p = 0.563$; 2 hr: $p = 0.173$; 6 hr, $p = 0.020$). As expected, the two models do equally well over short duration gaps, but as the gap between flights increases, the TC model does increasingly worse in predicting the relationship between the headings of the first and second flights. Thus, our experiments suggest that *Drosophila* do not compensate their sky compass to adjust for the azimuthal motion of the sun.

The finding that flies remember their flight heading for at least 2 hr makes ethological sense. *Drosophila* are crepuscular, exhibiting dawn and dusk activity peaks [27]. Assuming that our laboratory measurements are representative of dispersal events, a memory that allows an individual to fly straight for a few hours would be sufficient to bias a day's migration in one direction. To our knowledge, there is no evidence that *Drosophila* make multi-day, long-distance migrations that would require the ability to maintain a constant course from one day to the next or a TC sun compass. The most parsimonious ecological interpretation of their sun orientation behavior is that it allows flies to disperse opportunistically to new sources of food and oviposition sites within a single day.

The visual information conveying sun position likely provides inputs to the recently identified neurons constituting the fly's internal compass [17–19]. These columnar neurons receive input in the ellipsoid body and send divergent output to the protocerebral bridge and gall, and they are, hence, named E-PG neurons [28]. These neurons track the azimuthal position of vertical stripes and more complex visual stimuli and, in the absence of visual input, can continue to track azimuthal orientation by integrating estimates of angular velocity [17–19, 29]. Given these functional attributes, two obvious questions are whether E-PG neurons respond to a sun stimulus and whether they exhibit different responses to other visual stimuli. We used the split-GAL4 line SS00096 [29], which expresses in the E-PG neurons, to drive the genetically encoded calcium indicator GCaMP6f and measured activity in tethered, flying flies using a 2-photon microscope (Figure 2A). As described previously, the E-PG neurons tile the toroidally shaped ellipsoid body. Notably, a region of activity, or "bump," rotates around the ellipsoid body corresponding to azimuthal position ([17] Videos S1 and S2). Instead of recording from the ellipsoid body, we imaged the activity at E-PG terminals in the protocerebral bridge (Figure 2B), because fluorescence signals were stronger in these more superficial glomeruli. Based on well-established anatomy, we re-mapped the neural activity in the medial 16 glomeruli of the protocerebral bridge into the circular reference frame of the ellipsoid body (Figure 2C; [28]) and computed a neural activity vector average, or

(H) Polar representation of second sun-bout headings, plotted as in Figure 1D. Shaded area indicates sector that was not visible to fly.
(I) E-PG bump-to-stimulus offset for the second sun trial plotted against the mean sun heading.
(J) Regression of the median bump-to-stimulus offset for the second sun trial plotted against the offset for the first sun trial.
(K) Bump-to-stimulus offset for stripe plotted against the offset for the sun.
See also Videos S1 and S2.

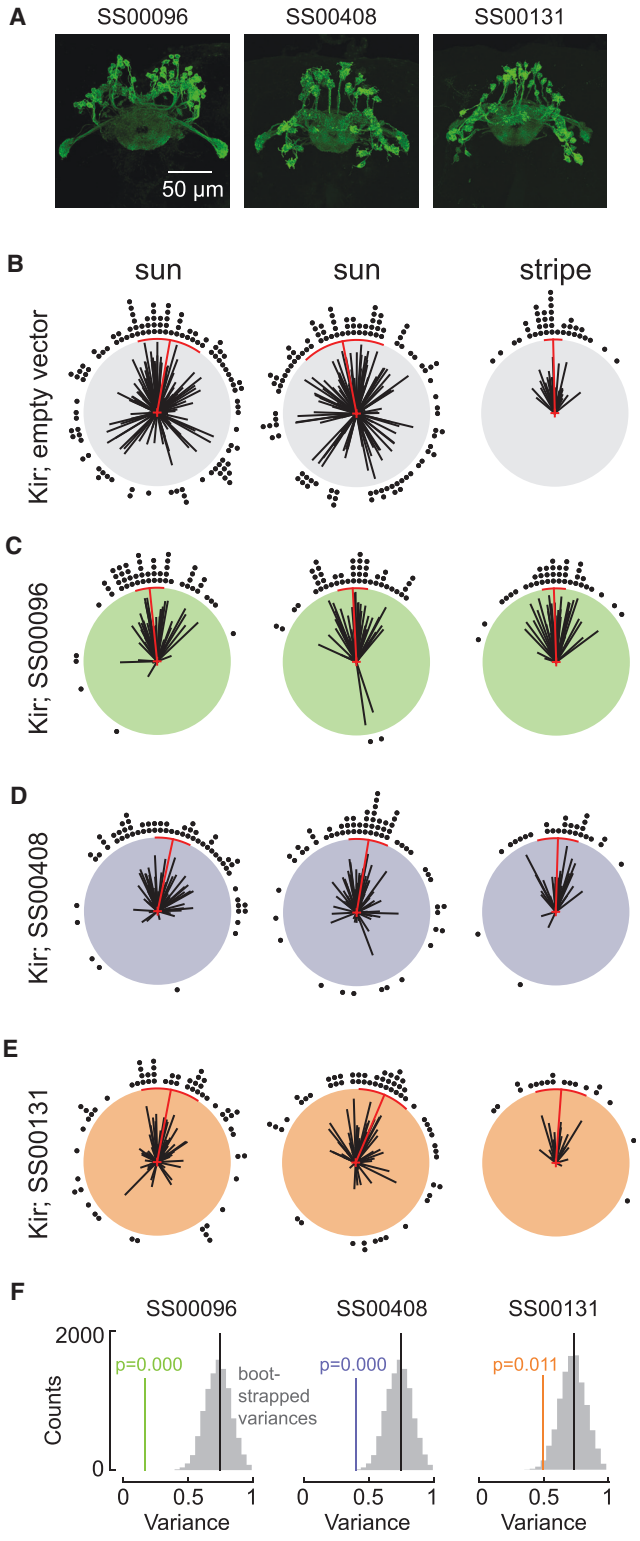

Figure 3. E-PG Neuron Activity Is Necessary for Sun Menotaxis

(A) Fluorescence labeling of GFP expressed in E-PG neurons in three experimental split-GAL4 lines, maximum-intensity projections. The exact number of E-PG neurons is not known, but we counted a range of 53–68 cells in the three driver lines used. Collectively, these cells tile all 16 medial glomeruli of the protocerebral bridge and all wedges of the ellipsoid body.

bump position, for each image (similar to [29]; see STAR Methods for details).

As in our flight arena experiments (Figure 1A), flies adopted arbitrary headings with respect to the sun stimulus (Figures 2G and 2H), which they maintained over a 5-min break (Figure 2G). By presenting sun and stripe stimuli to the same fly, we tested whether these two stimulus types are represented differently by the E-PG neurons. Bump position faithfully tracked the position of both the sun and stripe stimuli (Figures 2D–2F). Prior studies found that, while the E-PG bump tracks the azimuthal position of a vertical stripe, it does so with an arbitrary azimuthal angular offset [17]. We found an identical result with the sun stimulus; the bump rotated with changes in sun position but with a bump-to-stimulus offset that varied from individual to individual. In addition, the bump-to-stimulus offset did not differ between the first and second sun presentation trials or between the sun and stripe presentation trials (Figures 2J and 2K). The offset was not correlated with the azimuthal angle at which individual flies tended to hold the sun (Figure 2I). Together, these imaging results suggest that the representation of the sun and stripe in the E-PG neurons is similar, despite the distinct behavioral responses to the stimuli, and that the bump-to-stimulus offset does not encode heading preference.

We next tested the causal contributions of E-PG neurons to sun navigation and stripe fixation, predicting that the highly variable headings adopted in sun navigation might require the instantaneous positional information provided by E-PG neurons. We took advantage of the sparse expression patterns of three different split-GAL4 lines (Figure 3A) to selectively drive the inwardly rectifying potassium channel Kir2.1 [30]. As a control, we crossed UAS-Kir2.1 to an engineered split-GAL4 line that was genetically identical to the experimental driver lines but carried empty vectors of the two GAL4 domains in the two insertion sites [31]. Driving Kir2.1 in three separate split-GAL4 lines yielded flies that lost the ability to maintain the sun at arbitrary azimuthal positions, although they could fixate the sun and stripe frontally (Figures 3B–3F). To statistically assess whether flies with silenced E-PG neurons differed in heading distribution for the sun or stripe presentation, we conducted multisample Mardia-Watson-Wheeler tests for the first sun trial, the second sun trial, and the stripe presentation. Results from trials with stripes were not different across controls and experimental groups ($W = 10.625$, $p = 0.101$); however, we did detect differences in the distributions of data from the first and second sun stimulus trials (first trial: $W = 29.91$, $p < 0.0001$; second trial: $W = 41.39$,

(B) Sun menotaxis and stripe fixation in genetic controls (Kir; empty vector split-GAL4). Left: first 5-min trial of sun fixation (n = 111 flies). Center: second 5-min trial of sun fixation (n = 108). Right: 5 min of stripe fixation (n = 38).

(C) Results from the same experimental paradigm for Kir; SS00096 (ns = 54, 49, and 28).

(D) Sun and stripe fixation for Kir; SS00408 (ns = 64, 66, and 28).

(E) Headings from Kir; SS00131 (ns = 60, 60, and 19).

(F) Flies with silenced E-PG neurons have smaller variances than the genetic control. Distribution of 10,000 bootstrapped circular variances subsampled from the empty-vector control second sun trial are indicated in gray (n = 50 each). Black lines depict the observed heading variance of the entire dataset (n = 108). Colored lines indicate population heading variance of the second sun trial for each experimental group. The p values indicate the proportion of bootstrapped variances that are smaller than the observed variance for each experimental group.

$p < 0.0001$). To assess whether this result was due to differences in variance across control and E-PG-silenced flies, we used a bootstrapping approach similar to that used in our time gap experiments. We randomly sampled 50 values from our control dataset 10,000 times, in each case calculating the circular variance of the subsampled population. We then determined the proportion of bootstrapped mean variances that had smaller values than the variance of the actual experimental data and concluded that the observed frontal distributions of our experimental groups were highly unlikely to have occurred by chance (Figure 3F, SS00096: $p = 0.000$; SS00408: $p = 0.000$; SS00131: $p = 0.011$). Performing the analysis using the first sun trials gave almost identical results, except for the SS00131 line, in which the bootstrapped probability value was higher (SS00096: $p = 0.000$; SS00408: $p = 0.000$; SS00131: $p = 0.098$). We suspect that the consistently smaller effect using the SS00131 driver is due to weaker expression in this line. In summary, E-PG neuron activity appears necessary for menotaxis, i.e., maintaining the sun in arbitrary non-frontal positions. To our knowledge, this is the first behavioral deficit elicited via experimental manipulation of the compass cell network.

DISCUSSION

In the absence of normal E-PG function, flies might directly orient toward the sun, because they lack the ability to compare their instantaneous heading to a stored value of their directional preference. Such a loss of function in the compass network might unmask a simpler reflexive behavior, such as phototaxis, that does not require the elaborate circuitry of the central complex. Consistent with this hypothesis, stripe fixation was not different between control and experimental animals. This interpretation is compatible with a recent model that showed that frontal object fixation could result from a simple circuit involving two asymmetric wide-field motion integrators, without the need for the central complex [32].

Our findings are consistent with an emerging model of a navigational circuit involving the central complex. E-PG cells have an excitatory relationship with another cell class in the central complex (protocerebral bridge to ellipsoid body and noduli, or P-EN, neurons), creating an angular velocity integrator that allows a fly to maintain its heading in the absence of visual landmarks [18, 19]. Furthermore, the E-PG neurons are homologous to the CL1 neurons described in locusts [33], monarchs [16], dung beetles [4], and bees [34] and likely serve similar functions across taxa. Extracellular recordings from the central complex in cockroaches revealed neurons that act as head-direction cells relative to, or in the absence of, visual landmarks, although precise cell types were not identified [35]. Inputs to E-PG neurons likely occur via the anterior visual pathway from the medulla to the anterior optic tubercle and on to the bulb [36]. From there, tubercle-bulb neurons, one class of which is responsive to the azimuth and elevation of small bright spots, synapse onto ring neurons that project to the ellipsoid body, thus bringing visual information into the compass network [36]. In a recent model of path integration in bees, CL1 neurons are part of a columnar circuit that provides instantaneous heading information to an array of self-excitatory networks that also receive convergent optic flow information, thereby storing a memory of distance traveled in each direction [34]. This information is then retrieved as an animal returns home, by driving appropriate steering commands in another class of central complex neurons. The putative memory cells suggested by this model, CPU4 cells, could be homologous to protocerebral bridge-fan-shaped-body noduli (P-FN) neurons described for *Drosophila* [28]. Furthermore, cells responsive to progressive optic flow are found throughout the central complex of flies, including neuropil in the fan-shaped body containing the P-FN cells [37]. In addition to their role in path integration, the CPU4 network might also function to store the desired heading during sun navigation [34, 38]. Although our results do not directly test this model, they are consistent with the role of CL1 neurons in providing heading direction to circuits that generate steering commands toward an arbitrary orientation whose memory is stored in the network of CPU4 (P-FN) neurons.

Stripe fixation and sun navigation behaviors may represent two different flight modes in *Drosophila.* Stripe fixation is thought to be a short-range behavioral reflex to orient toward near objects [12], which, in free flight, is quickly terminated by collision avoidance [13] or landing behaviors [39]. In contrast, navigation using the sun is likely a component of long-distance dispersal behavior that could be used in conjunction with polarization vision [8, 9] either in a hierarchical [4] or integrative [40] manner. Individuals could differ in where they lie on the continuum of long-range dispersal to local search, which could explain the inter-individual variation we observed in heading fidelity during sun orientation experiments. In general, dispersal is a condition-dependent behavior that is known to vary with hunger or other internal factors [41]. Given the architectural similarity of the central complex among species [42], the celestial compass we have identified in *Drosophila* is likely one module within a conserved behavioral toolkit [13], allowing orientation and flight over long distances by integrating skylight polarization, the position of the sun or moon, and other visual cues. An independent study has recently found that the E-PG compass neurons are also necessary in walking flies for maintaining arbitrary headings relative to a small bright object [43]. The expanding array of genetic tools developed for flies and the rapid growth in our understanding of the neural circuitry involved in orientation during walking [17–19] and flight [29] make this a promising system for exploring such essential and highly conserved behaviors.

STAR★METHODS

Detailed methods are provided in the online version of this paper and include the following:

- KEY RESOURCES TABLE
- CONTACT FOR REAGENT AND RESOURCE SHARING
- EXPERIMENTAL MODEL AND SUBJECT DETAILS
- METHOD DETAILS
  - Fly tethering
  - Flight arenas and stimulus presentation
  - Sun orientation and time gap experiments
  - 2-photon functional imaging
  - Functional silencing of E-PG neurons in sun navigation behavior
  - Immunohistochemistry of split-GAL4 lines
- QUANTIFICATION AND STATISTICAL ANALYSIS
- DATA AND SOFTWARE AVAILABILITY

SUPPLEMENTAL INFORMATION

Supplemental Information includes two videos and can be found with this article online at https://doi.org/10.1016/j.cub.2018.07.002.

ACKNOWLEDGMENTS

We thank Tanya Wolff and Gerry Rubin for generously providing us with the split-GAL4 lines SS00131 and SS00408 prior to the publication of their manuscript describing them. Crystal Liang and Aisling Murran provided valuable assistance with data collection. This work was funded by grants from the NSF (IOS 1547918), NIH (U19NS104655), and the Simons Foundation (71582123) to M.H.D., as well as an NIH NRSA postdoctoral fellowship (F32GM109777) to Y.M.G.

AUTHOR CONTRIBUTIONS

P.T.W. and T.L.W. were involved in early experimental design and collected preliminary data on sun orientation behavior. Y.M.G., K.J.L., I.G.R., and M.H.D. conceived of and conducted experiments. Y.M.G. characterized sun compass behavior (Figure 1), I.G.R. conducted functional imaging experiments (Figure 2), and Y.M.G. and K.J.L. performed genetic silencing experiments (Figure 3). Y.M.G., K.J.L., I.G.R., and M.H.D. wrote the paper. All authors contributed in editing the final manuscript.

DECLARATION OF INTERESTS

The authors declare no competing interests.

Received: June 6, 2018
Revised: June 28, 2018
Accepted: July 2, 2018
Published: August 30, 2018

REFERENCES

1. Åkesson, S., and Wehner, R. (2002). Visual navigation in desert ants *Cataglyphis fortis*: are snapshots coupled to a celestial system of reference? J. Exp. Biol. *205*, 1971–1978.
2. Fent, K. (1986). Polarized skylight orientation in the desert ant *Cataglyphis*. J. Comp. Physiol. A Neuroethol. Sens. Neural Behav. Physiol. *158*, 145–150.
3. Lebhardt, F., and Ronacher, B. (2014). Interactions of the polarization and the sun compass in path integration of desert ants. J. Comp. Physiol. A Neuroethol. Sens. Neural Behav. Physiol. *200*, 711–720.
4. el Jundi, B., Warrant, E.J., Byrne, M.J., Khaldy, L., Baird, E., Smolka, J., and Dacke, M. (2015). Neural coding underlying the cue preference for celestial orientation. Proc. Natl. Acad. Sci. USA *112*, 11395–11400.
5. el Jundi, B., Smolka, J., Baird, E., Byrne, M.J., and Dacke, M. (2014). Diurnal dung beetles use the intensity gradient and the polarization pattern of the sky for orientation. J. Exp. Biol. *217*, 2422–2429.
6. Reppert, S.M., Guerra, P.A., and Merlin, C. (2016). Neurobiology of monarch butterfly migration. Annu. Rev. Entomol. *61*, 25–42.
7. Homberg, U., Heinze, S., Pfeiffer, K., Kinoshita, M., and el Jundi, B. (2011). Central neural coding of sky polarization in insects. Philos. Trans. R. Soc. Lond. B Biol. Sci. *366*, 680–687.
8. Warren, T.L., Weir, P.T., and Dickinson, M.H. (2018). Flying *Drosophila melanogaster* maintain arbitrary but stable headings relative to the angle of polarized light. J. Exp. Biol. *221*, jeb177550.
9. Weir, P.T., and Dickinson, M.H. (2012). Flying *Drosophila* orient to sky polarization. Curr. Biol. *22*, 21–27.
10. Wehner, R., and Müller, M. (2006). The significance of direct sunlight and polarized skylight in the ant's celestial system of navigation. Proc. Natl. Acad. Sci. USA *103*, 12575–12579.
11. Coyne, J.A., Boussy, I.A., Prout, T., Bryant, S.H., Jones, J.S., and Moore, J.A. (1982). Long-distance migration of *Drosophila*. Am. Nat. *119*, 589–595.
12. Götz, K.G. (1987). Course-control, metabolism and wing interference during ultralong tethered flight in *Drosophila melanogaster*. J. Exp. Biol. *128*, 35–46.
13. Dickinson, M.H. (2014). Death Valley, *Drosophila*, and the Devonian toolkit. Annu. Rev. Entomol. *59*, 51–72.
14. el Jundi, B., Pfeiffer, K., and Homberg, U. (2011). A distinct layer of the medulla integrates sky compass signals in the brain of an insect. PLoS ONE *6*, e27855.
15. Pegel, U., Pfeiffer, K., and Homberg, U. (2018). Integration of celestial compass cues in the central complex of the locust brain. J. Exp. Biol. *221*, jeb171207.
16. Heinze, S., and Reppert, S.M. (2011). Sun compass integration of skylight cues in migratory monarch butterflies. Neuron *69*, 345–358.
17. Seelig, J.D., and Jayaraman, V. (2015). Neural dynamics for landmark orientation and angular path integration. Nature *521*, 186–191.
18. Turner-Evans, D.B., Wegener, S., Rouault, H., Franconville, R., Wolff, T., Seelig, J.D., Druckmann, S., and Jayaraman, V. (2017). Angular velocity integration in a fly heading circuit. eLife *6*, e23496.
19. Green, J., Adachi, A., Shah, K.K., Hirokawa, J.D., Magani, P.S., and Maimon, G. (2017). A neural circuit architecture for angular integration in *Drosophila*. Nature *546*, 101–106.
20. Taube, J.S. (2007). The head direction signal: origins and sensory-motor integration. Annu. Rev. Neurosci. *30*, 181–207.
21. Hoyer, S.C., Eckart, A., Herrel, A., Zars, T., Fischer, S.A., Hardie, S.L., and Heisenberg, M. (2008). Octopamine in male aggression of *Drosophila*. Curr. Biol. *18*, 159–167.
22. Reichardt, W., and Poggio, T. (1976). Visual control of orientation behaviour in the fly. Part I. A quantitative analysis. Q. Rev. Biophys. *9*, 311–438.
23. Maimon, G., Straw, A.D., and Dickinson, M.H. (2008). A simple vision-based algorithm for decision making in flying *Drosophila*. Curr. Biol. *18*, 464–470.
24. Wolf, R., Gebhardt, B., Gademann, R., and Heisenberg, M. (1980). Polarization sensitivity of course control in *Drosophila melanogaster*. J. Comp. Physiol. A Neuroethol. Sens. Neural Behav. Physiol. *139*, 177–191.
25. el Jundi, B., Foster, J.J., Khaldy, L., Byrne, M.J., Dacke, M., and Baird, E. (2016). A snapshot-based mechanism for celestial orientation. Curr. Biol. *26*, 1456–1462.
26. Blewitt, M. (2017). Celestial Navigation for Yachtsmen, 13th edition (Adlard Coles Nautical).
27. Rieger, D., Fraunholz, C., Popp, J., Bichler, D., Dittmann, R., and Helfrich-Förster, C. (2007). The fruit fly *Drosophila melanogaster* favors dim light and times its activity peaks to early dawn and late dusk. J. Biol. Rhythms *22*, 387–399.
28. Wolff, T., Iyer, N.A., and Rubin, G.M. (2015). Neuroarchitecture and neuroanatomy of the *Drosophila* central complex: A GAL4-based dissection of protocerebral bridge neurons and circuits. J. Comp. Neurol. *523*, 997–1037.
29. Kim, S.S., Rouault, H., Druckmann, S., and Jayaraman, V. (2017). Ring attractor dynamics in the *Drosophila* central brain. Science *356*, 849–853.
30. Baines, R.A., Uhler, J.P., Thompson, A., Sweeney, S.T., and Bate, M. (2001). Altered electrical properties in *Drosophila* neurons developing without synaptic transmission. J. Neurosci. *21*, 1523–1531.
31. Hampel, S., Franconville, R., Simpson, J.H., and Seeds, A.M. (2015). A neural command circuit for grooming movement control. eLife *4*, e08758.
32. Fenk, L.M., Poehlmann, A., and Straw, A.D. (2014). Asymmetric processing of visual motion for simultaneous object and background responses. Curr. Biol. *24*, 2913–2919.
33. Heinze, S., and Homberg, U. (2009). Linking the input to the output: new sets of neurons complement the polarization vision network in the locust central complex. J. Neurosci. *29*, 4911–4921.
34. Stone, T., Webb, B., Adden, A., Weddig, N.B., Honkanen, A., Templin, R., Wcislo, W., Scimeca, L., Warrant, E., and Heinze, S. (2017). An

anatomically constrained model for path integration in the bee brain. Curr. Biol. *27*, 3069–3085.e11.

35. Varga, A.G., and Ritzmann, R.E. (2016). Cellular basis of head direction and contextual cues in the insect brain. Curr. Biol. *26*, 1816–1828.
36. Omoto, J.J., Keleş, M.F., Nguyen, B.M., Bolanos, C., Lovick, J.K., Frye, M.A., and Hartenstein, V. (2017). Visual input to the *Drosophila* central complex by developmentally and functionally distinct neuronal populations. Curr. Biol. *27*, 1098–1110.
37. Weir, P.T., and Dickinson, M.H. (2015). Functional divisions for visual processing in the central brain of flying *Drosophila*. Proc. Natl. Acad. Sci. USA *112*, E5523–E5532.
38. Heinze, S. (2017). Unraveling the neural basis of insect navigation. Curr. Opin. Insect Sci. *24*, 58–67.
39. Borst, A. (1990). How do flies land? From behavior to neuronal circuits. Bioscience *40*, 292–299.
40. Wehner, R., Hoinville, T., Cruse, H., and Cheng, K. (2016). Steering intermediate courses: desert ants combine information from various navigational routines. J. Comp. Physiol. A Neuroethol. Sens. Neural Behav. Physiol. *202*, 459–472.
41. Dingle, H. (1996). Migration: The Biology of Life on the Move (Oxford University Press).
42. Strausfeld, N.J. (2012). Arthropod Brains: Evolution, Functional Elegance, and Historical Significance (Belknap Press).
43. Green, J., Vijayan, V., Mussells-Pires, P., Adachi, A., and Maimon, G. (2018). Walking *Drosophila* aim to maintain a neural heading estimate at an internal goal angle. bioRxiv. https://doi.org/10.1101/315796.
44. Clark, M.Q., McCumsey, S.J., Lopez-Darwin, S., Heckscher, E.S., and Doe, C.Q. (2016). Functional genetic screen to identify interneurons governing behaviorally distinct aspects of *Drosophila* larval motor programs. G3 (Bethesda) *6*, 2023–2031.
45. Chen, T.W., Wardill, T.J., Sun, Y., Pulver, S.R., Renninger, S.L., Baohan, A., Schreiter, E.R., Kerr, R.A., Orger, M.B., Jayaraman, V., et al. (2013). Ultrasensitive fluorescent proteins for imaging neuronal activity. Nature *499*, 295–300.
46. Maimon, G., Straw, A.D., and Dickinson, M.H. (2010). Active flight increases the gain of visual motion processing in *Drosophila*. Nat. Neurosci. *13*, 393–399.
47. *Drosophila* adult hemolymph-like saline (AHLS) (2013). Cold Spring Harb. Protoc. 10.1101/pdb.rec079459.
48. Reiser, M.B., and Dickinson, M.H. (2008). A modular display system for insect behavioral neuroscience. J. Neurosci. Methods *167*, 127–139.
49. David, C.T. (1978). The relationship between body angle and flight speed in free-flying *Drosophila*. Physiol. Entomol. *3*, 191–195.
50. Suver, M.P., Huda, A., Iwasaki, N., Safarik, S., and Dickinson, M.H. (2016). An array of descending visual interneurons encoding self-motion in *Drosophila*. J. Neurosci. *36*, 11768–11780.
51. Heisenberg, M., and Wolf, R. (1984). Vision in *Drosophila*: Genetics of Microbehavior (Springer-Verlag).
52. Nern, A., Pfeiffer, B.D., and Rubin, G.M. (2015). Optimized tools for multicolor stochastic labeling reveal diverse stereotyped cell arrangements in the fly visual system. Proc. Natl. Acad. Sci. USA *112*, E2967–E2976.
53. Schindelin, J., Arganda-Carreras, I., Frise, E., Kaynig, V., Longair, M., Pietzsch, T., Preibisch, S., Rueden, C., Saalfeld, S., Schmid, B., et al. (2012). Fiji: an open-source platform for biological-image analysis. Nat. Methods *9*, 676–682.
54. Schneider, C.A., Rasband, W.S., and Eliceiri, K.W. (2012). NIH Image to ImageJ: 25 years of image analysis. Nat. Methods *9*, 671–675.
55. Hunter, J.D. (2007). Matplotlib: A 2D graphics environment. Comput. Sci. Eng. *9*, 90–95.
56. Zarr, J.H. (1999). Biostatistical Analysis (Prentice Hall).
57. Berens, P. (2009). CircStat: A MATLAB Toolbox for Circular Statistics. J. Stat. Softw. *31*, 1–21.

STAR★METHODS

KEY RESOURCES TABLE

REAGENT or RESOURCE	SOURCE	IDENTIFIER
Antibodies		
AlexaFluor488-conjugated rabbit anti-tag IgG	ThermoFisher Scientific	A-21311; RRID: AB_221477
Mouse mAb anti-Bruchpilot (nc82)	Developmental Studies Hybridoma Bank	nc82; RRID: AB_2314866
AlexaFluor633-conjugated goat anti-mouse IgG	ThermoFisher Scientific	A-21050; RRID_2535718
Deposited Data		
Raw and analyzed data	This paper	https://doi.org/10.17632/gbj3fx9f58.1
Experimental Models: Organisms/Strains		
D. melanogaster: SS00096-SplitGAL4 (*P{w[+mc]=GMR19G02-pBPp65ADZpUw}* in *attP40* and *P{w[+mc]=GMR70G12-pBPZpGDBDUw}* in *attP2*)	Gift from V. Jayaraman [29]	N/A
D. melanogaster: SS00131-SplitGAL4	Gift from T. Wolff (Janelia Research Campus)	N/A
D. melanogaster: SS00408-SplitGAL4	Gift from T. Wolff (Janelia Research Campus)	N/A
D. melanogaster: Empty-SplitGAL4 (*P{w[+mc]=BP-p65ADZp}* in *attP40}* and *P{w[+mc]=BP-ZpG4DBD}* in *attP2*)	Gift from J. Simpson [31]	N/A
D. melanogaster: ;UAS-OpGCaMP6f (*20XUAS-IVS-Syn21-OpGCamp6F-p10* in *attP5*)	Gift from D. Anderson	N/A
D. melanogaster: ;UAS-tdTomato (*P{w[+mC] = UAS-tdTom.S}3*)	Bloomington Drosophila Stock Center	RRID:BDSC_36328
D. melanogaster: ;UAS-OpGCaMP6f; UAS-tdTomato	Constructed from above two lines	N/A
D. melanogaster: ;;UAS-myr::GFP (*10xUAS-IVS-myr::GFP* in *attP40*)	Bloomington Drosophila Stock Center	RRID:BDSC_32197
D. melanogaster: ;;UAS-RedStinger (*w[+mC] = UAS-RedStinger*)	Bloomington Drosophila Stock Center	RRID:BDSC_8547
D. melanogaster: ;;UAS-myr::GFP,UAS-RedStinger	Gift from M.Q. Clark [44], constructed from two lines above	N/A
D. melanogaster: +;+;UAS-eGFP-Kir2.1 (*pJFRC49-10XUAS-IVS-eGFPKir2.1* in *attP2*)	Gift from W. Korff, G. Card, and H. Namiki (Janelia Research Campus)	N/A
Software and Algorithms		
Python 2.7	https://www.python.org	RRID:SCR_008394
Matplotlib	https://matplotlib.org	RRID:SCR_008624
astropy.stats.cirstats python module	http://docs.astropy.org/en/stable/stats/circ.html#module-astropy.stats.circstats	N/A
circstats.py python module	https://github.com/jhamrick/python-snippets/blob/master/snippets/circstats.py	N/A
FIJI	NIH (https://fiji.sc/)	RRID:SCR_002285
Oriana	https://www.kovcomp.co.uk/oriana/	N/A

CONTACT FOR REAGENT AND RESOURCE SHARING

Further information and requests for resources and reagents should be directed to and will be fulfilled by the Lead Contact, Michael Dickinson (flyman@caltech.edu).

EXPERIMENTAL MODEL AND SUBJECT DETAILS

We conducted all experiments using 2-4 day old female *Drosophila melanogaster.* Our initial analysis of sun orientation behavior (Figure 1) was conducted using flies from a wild-caught strain ('top banana') collected in Seattle, WA and maintained in the lab since September 2013. We reared flies in incubators on a 12 hour light: 12 hour dark cycle at 25°C on standard cornmeal fly food. For the functional imaging experiments (Figure 2), we used flies heterozygous for w+;UAS-tdTomato;UAS-GCaMP6f [45] and the split-Gal4 line SS00096 [29]. For silencing experiments (Figure 3), we crossed a backcrossed version of UAS-Kir2.1 with SS00096, SS00131, and SS00408 (kindly provided by Tanya Wolff at Janelia Research Campus). The controls in our silencing experiments were the progeny of the UAS-Kir2.1 line and an engineered split-GAL4 line in which the two insertion sites carried empty vectors of the two GAL4 domains, but were otherwise genetically identical to the experimental driver lines [31]. We generated flies for confocal imaging by crossing UAS-myr:GFP,UAS-red-Stinger with each of the split-GAL4 lines.

METHOD DETAILS

Fly tethering

For sun orientation (Figure 1) and genetic silencing experiments (Figure 3), we tethered flies under cold anesthesia and glued them to a tungsten wire (0.13 mm diameter) at the anterior dorsal portion of the scutum with UV-cured glue (Bondic Inc.). We also fixed the head of each fly to its thorax by applying an additional drop of glue. Flies were allowed to recover for at least 10 minutes prior to testing.

For functional imaging experiments (Figure 2), we tethered each fly to a specially designed physiology stage [46] that permitted access to the posterior side of the fly's head. We filled the holder with saline, and removed a section of cuticle overlying the region of the central complex. To improve imaging quality, we removed adipose bodies and the trachea from the light path. Flies were continuously perfused with saline [47] which was actively regulated to a temperature of 21°C. We allowed flies a minimum of 20 minutes to recover from cold-anesthesia prior to imaging.

Flight arenas and stimulus presentation

For sun-orientation behavior (Figure 1) and genetic silencing experiments (Figure 3), we placed tethered flies in an LED flight simulator [48] (Figure 1A). We displayed patterns on a circular arena of either 12 × 1 (Figure 1) or 12 × 2 (Figure 3) LED panels, with each panel consisting of an 8 × 8 array of individual pixels (Betlux #BL-M12A881PG-11, $\lambda = 525$ nm). Each pixel subtended an angle of 2.8° at the center of the arena with a 0.93° gap between adjacent pixels. The panels were controlled using hardware and firmware (IORodeo.com) as described previously [48], with slight modifications in current sinking required to display a single bright pixel without generating bleed-through on other pixels in the same panel row. We placed the fly in the center of the arena at a body angle of ~60°, approximating the orientation during free flight [49]. For wing tracking, flies were backlit with a collimated infrared source (850 nm, 900mW; Thorlabs Inc. #M850L3). We placed a 45° mirror below the fly and used a firewire camera (Basler A602f-2) or a Point Grey USB 3.0 camera (now FLIR, Blackfly 0.3MP monochrome camera, BFLY-U3-03S2M-CS) for image capture. Each camera was equipped with a Computar macro lens (MLM3X-MP) and IR-pass filter (Hoya B-46RM72-GB) to exclude extraneous light from the LED display.

To track the wing stroke envelope during flight, we used Kinefly, real-time machine-vision software developed in the lab [50]. As in previous studies [12], we used the difference in wing beat amplitude (ΔWBA) as a feedback signal by which the fly could control the azimuthal angular velocity of the visual stimulus. The gain of this control relationship was set to 14.67, 5.88, or 4.75° sec^{-1} for each °ΔWBA for sun orientation experiments (Figure 1), functional imaging (Figure 2), and genetic silencing (Figure 3), respectively. We found that a lower feedback gain was required in our experiments with transgenic lines to generate stable orientation behavior to both sun and stripe stimuli.

For functional imaging experiments, we presented visual stimuli using a 12 × 4 panel (96 × 32 pixel) arena, which covered 216° of azimuth with a resolution of ~2.25° $pixel^{-1}$. To reduce light pollution from the LED arena into the photomultiplier tubes of the 2-photon microscope, we shifted the spectral peak of the visual stimuli from 470 nm to 450 nm by placing two transmission filters in front of the LEDs (Roscolux no. 59 Indigo and no. 39 Skelton Exotic Sangria). We tracked wing beat angles using Kinefly and presented stimuli in closed-loop as described above, except that we illuminated the wings using four horizontal fiber-optic IR light sources (Thorlabs Inc. #M850F2) distributed in a ~90° arc behind the fly.

For data presented in Figures 1 and 3, a single pixel served as our ersatz sun. At the plane of the fly, a single pixel subtends a maximum angle of 2.8°. However, because the fly was placed ~30° below the plane of the illuminated pixel, the simulated sun subtended a maximum angle of ~2.4° at the fly's retina, which is larger than the sun's angular diameter (~0.5°), but smaller than the inter-ommatidial acceptance angle of ~5° [51]. For sun orientation experiments (Figure 1), we conducted all trials in a 12 × 1 panel (96 × 8 pixel) arena. For stripe fixation, we presented a 4 pixel-wide dark stripe (15° wide x 30° high) on a bright background.

To determine the visual contrast flies experienced during our experiments, we measured the normalized difference between the lightest and darkest parts of the display (Michelson contrast). We placed a small metal tube covered in black electrical tape over a power sensor (Thorlabs S170C, PM100D) to reduce reflections and approximate the acceptance angle of an ommatidium (~5°). We held the sensor at the center of the arena and directed it toward a sun or stripe to measure the stimulus light level and then moved

the stimulus 45° in azimuth to measure the background light level. The Michelson contrast for all sun stimulus experiments was 0.99 and stripe contrast was 0.75 and 0.74 for the data presented in Figure 1 and Figure 3 respectively.

The behavior of flies from the control line (UAS-Kir;split-GAL4-empty-vector) was generally similar to wild-type flies; however, they tended to perform poorly in the stripe-fixation paradigm, as indicated by relatively low vector strength (Figure 3B) and a smaller proportion of flies that completed the trial without stopping. Given that flies' azimuthal control of a stripe stimulus improves as a function of increasing stripe height [23], we doubled the height of the visual display to a stripe of ~58° (12 × 2 panels, 96 × 16 pixels) for our genetic silencing experiments (Figure 3). We noted that reflections generated by a single bright pixel on the faceted inner surface of the arena generated a faint dark stripe on the column of panels on which the sun stimulus was displayed. To guard against the possibility that the fly would orient to this reflection feature, we fabricated cylindrical inserts of black velvet that obscured the surface of the display except for a narrow slit (9 mm x 360°) that contained the LED row in which the sun stimulus was displayed. The insert could be quickly removed without disturbing the fly for trials using a stripe stimulus. To facilitate the collection of large sample sizes for the genetic silencing experiments, we constructed two identical arenas, which we operated in parallel.

In the functional imaging experiments (Figure 2) we compensated for a larger arena and dimmer LEDs by using a 3.6° x 3.6° spot (2 × 2 pixels) as our sun stimulus, with a Michelson contrast of 0.92. During all experiments, the sun stimulus was presented to the flies at an inclination of 30°. The stripe stimulus consisted of a 12.6° wide x 64° high vertical bright stripe presented on a dark background, with a Michelson contrast of 0.93. Due to the sensitivity of the photomultipliers in the 2-photon microscope, we were constrained to display a bright stripe on a dark background rather than a dark stripe on a bright background; however, evidence suggests that flies response to these two stimuli in a similar fashion [48].

Sun orientation and time gap experiments

To test the persistence of flight headings, we presented flies with the sun stimulus in closed loop, provided a rest period between flights for either 5 minutes, 1 hour, 2 hours, or 6 hours, and then tested flies in a second bout with a sun stimulus. Before and after the sun stimulus trials, we presented flies with a stripe for 1 minute. For 5-minute inter-trial intervals, we left the fly in the arena and stopped flight by presenting a small piece of paper. To prevent dehydration during longer inter-trial intervals (1, 2 and 6 hours), we removed the fly from the arena and placed it on a small foam ball floating in a microcentrifuge tube filled with water. Following this rest period, we returned the fly to the arena and the second flight was initiated by providing a small puff of air. We discarded trials in which any fly stopped flying more than once during any of the stripe or sun presentations.

2-photon functional imaging

We imaged at an excitation wavelength of 930 nm using a galvanometric scan mirror-based two-photon microscope (Thorlabs, Inc., Newton, NJ, USA) equipped with a Nikon CFI Plan Fluorite objective water-immersion lens (10x mag., 0.3 N.A., 3.5 mm W.D.). With the addition of a piezo-ceramic linear objective drive (P-726, Physik Instrumente GmbH and Co. KG, Karlsruhe, Germany) we imaged two x-y planes separated by 25 μm along the z axis. Within the resulting volume we recorded tdTomato and GCaMP6f fluorescence in those glomeruli of the protocerebral bridge that contain terminals of E-PG neurons. We scanned in a boustrophedon pattern from ventral to dorsal to align the piezo drive descent during each plane scan with the anatomical inclination of the protocerebral bridge, maximizing the volumetric capture of the target glomeruli. We acquired the 142 × 71 μm images with 128 × 64 pixel resolution at 13.1 Hz. The 2-plane scan with one fly-back frame resulted in a 4.36 Hz volumetric scan rate. To correct for motion in the x-y plane, we registered both channels for each frame by finding the peak of the cross correlation between each tdTomato image and the trial-averaged image [37]. Subsequently, we collapsed the two planes with a maximum z-projection. Based on known anatomy, we manually assigned a region of interest (ROI) to each PB glomerulus with E-PG neuron innervation. For each volumetric frame, we computed fluorescence (F_t) of the GCaMP6f signal by subtracting the mean of the background pixels from the mean of the ROI pixels for each glomerulus. The background was defined as the 10% dimmest pixels across the entire z-projected image for each fly. We normalized the fluorescence in the ROI of each glomerulus to its baseline fluorescence (F_0) as follows: $\Delta F/F = (F_t - F_0)/F_0$ and defined F_0 as the mean of the 10% lowest GCaMP6f fluorescence in the ROI of each glomerulus. Under closed-loop conditions, we presented each fly with a sun stimulus twice for five minutes, separated by a minimum of 5 minutes. A 2-minute presentation of the stripe stimulus followed the second sun stimulus trial.

Functional silencing of E-PG neurons in sun navigation behavior

We tested all control and experimental flies with a paradigm consisting of 5 minutes of sun stimulus presentation, a 5-minute break, 5 minutes of sun presentation, and 5 minutes of stripe presentation. We discarded trials in which flies stopped more than twice per stimulus presentation.

Immunohistochemistry of split-GAL4 lines

We dissected and stained brains of flies expressing UAS-myr:GFP, UAS-redStinger and each of the three split-GAL4 lines (SS00096, SS00131, SS00408) using modifications to standard laboratory immunohistochemistry protocols [50]. We dissected brains in 4% formaldehyde fixative. After a 20-30 minute fixation, we washed tissue 2 × 20 minutes in phosphate buffered saline (PBS) followed by a permeabilization step of 2 × 20 minute washes in phosphate buffered saline with 0.5% Triton-X (PBST). We incubated tissue with primary antibodies anti-GFP AlexaFluor 488 conjugate (1:1000 concentration, Invitrogen # A21311) and anti-nc82 to label neuropil (1:10 concentration, Developmental Studies Hybridoma Bank, AB 2314866) in 5% normal goat serum in PBST overnight on a nutator

at 4°C. The following day, we washed with PBST 3 × 20 min and incubated with a secondary antibody to anti-nc82 (AlexaFluor 633, 1:250 concentration, Invitrogen # A21050) overnight at 4°C. Brains were washed 3 × 20 min with PBST and 2 × 20 min with PBS the following day. We dehydrated brains through an ethanol series (30%, 50%, 70%, 90%, 100%, 100%, each for 10 min), cleared tissue with xylene (2 × 10 min) and mounted in DPX [52]. Using a Leica SP8, we imaged brains under a 63x objective (Leica #506350, 1.4 N.A.). Maximum intensity projections were generated in Fiji [53, 54] and cell bodies were counted manually on the corresponding image stacks.

QUANTIFICATION AND STATISTICAL ANALYSIS

We processed and analyzed data in Python 2.7 and Matplotlib [55] unless otherwise noted below. We tested all datasets for non-uniformity using a Rayleigh test from the astropy.stats.circstats python module (http://docs.astropy.org/en/stable/stats/circ.html#module-astropy.stats.circstats). Circular mean and 95% confidence interval are shown on each polar plot. The 95% confidence interval was calculated using the circstats.py module (https://github.com/jhamrick/python-snippets/blob/master/snippets/circstats.py) using the formula provided by Zarr [56, 57]. Before making pairwise comparisons of mean heading direction in separate flights (as in Figures 1F–1H), we excluded trials with a vector strength under 0.2 (33% of all trials). Mean headings for flights with very low vector strength are not meaningful, as this indicates that the fly did not select a heading during the trial. However, including all data did not qualitatively change the relationship between first and second flights. For each time gap experiment, we selected the first stripe and first sun datasets and tested each pair for differences in heading distribution (Mardia-Watson-Wheeler test, Oriana, https://www.kovcomp.co.uk). The resultant p values were robust to whether or not we excluded data points with a mean vector strength cutoff of 0.2 (all p values less than 0.023).

To assess whether heading fidelity was maintained over time gaps, we bootstrapped random pairings of first and second sun presentation trials 10,000 times. We compared the distribution of the mean absolute value of heading difference between the flights for these simulated datasets to the mean absolute value of heading difference of the observed data (Figure 1H). We calculated the p value as the proportion of simulated datasets that had a mean heading difference smaller than that of the observed data. For our behavioral genetics experiments we asked whether genotypes differed in heading by performing a Watson-Wheeler-Mardia test (Oriana, https://www.kovcomp.co.uk). While there was no detectable difference for stripe presentation, we found significant differences for the sun stimulus, both when performed for the second flight and the first flight. To determine whether flies with silenced E-PGs differed from controls, we conducted a pairwise comparison similar to the one we conducted for the time gap experiments. In this case we bootstrapped subsamples (N = 50) of our control dataset with replacement 10,000 times and calculated the circular variance of each dataset. As above, we then reported the proportion of bootstrapped datasets with a smaller variance than the variance for each experimental group. We selected a resample size of 50 as this approximated the sample size of our datasets (N = 49, 66, 60). A systematic analysis of p values showed that they decreased asymptotically to a constant level at resample sizes greater than 20.

To assess whether the time gap data (Figure 1F) were better described by a time compensation (TC) model (which would predict a $15^{\circ}\ hr^{-1}$ directional shift in heading) or a fixed memory (FM) model, we subsampled (N = 20) without replacement from each dataset 10,000 times. From each subsample we calculated the difference in mean squared circular residuals (MSR) for the TC prediction and the FM prediction. We report for each dataset the proportion of subsampling iterations in which the TC MSR was less than the FM MSR, with lower p values indicating a better fit to the TC model.

DATA AND SOFTWARE AVAILABILITY

The data from this manuscript are published on Mendeley Data at https://doi.org/10.17632/gbj3fx9f58.1.